Electronic Supplementary Material (ESI) for CrystEngComm.

Supporting Information

Controllable and Defectless Cutting Postprocess Method via Cleavage of an Elastic Cocrystal Based on Pyrene and Tetrachloroterephthalonitrile

Xu Yu, Baolei Tang and Hongyu Zhang*

State Key Laboratory of Supramolecular Structure and Materials, College of Chemistry, Jilin University, Changchun 130012, P. R. China.

E-mail: hongyuzhang@jlu.edu.cn

Contents

1. General Information

1.1 Materials and Reagents

Starting materials for organic syntheses were obtained from commercial sources and used as received.

1.2 Experimental Section

1.2.1 Crystal Growth

Dissolve equal molar compounds in dichloromethane to produce a saturated solution. Add 1 mL saturated solution into each of the three glass tubes separately. Then, add 2 mL ethanol into glass tubes, along the tube wall without destroying the previous solution surface and then seal the tube with parafilm. Two different organic phases gradually diffused with each other as time went by. After standing at room temperature for about 14 days, crystals were obtained.

1.2.2 Spectra

Uv-vis absorption spectra were recorded by a Shimadzu UV-2550 spectrophotometer. Emission spectra were recorded by a Shimadzu RF-5301 PC spectrometer or a Maya2000 Pro CCD spectrometer. The absolute fluorescence quantum yield was measured on an Edinburgh FLS920 spectrometer combined with a calibrated integrating sphere. Fluorescence lifetimes were measured on an Edinburgh FLS920 using a time-correlated single-photon (TCSPC) module. Edge emission and PL spectra of the crystals were detected using a Maya2000 Pro CCD spectrometer. All the measurements were carried out at room temperature under ambient conditions.

1.2.3 X-ray Crystallographic Analysis

Single crystal X-ray diffraction data were collected on a Rigaku RAXIS-PRID diffractometer using the ω-scan mode with graphite-monochromator Mo•Kα radiation. Structures were solved with direct methods using the SHELXTL programs and refined with full-matrix least-squares on F2. Non-hydrogen atoms were refined anisotropically. Positions of hydrogen atoms were calculated and refined isotropically. The crystallographic information was deposited at the Cambridge Crystallographic Data Centre (CCDC). CCDC number: 2084307, 2084309. The crystal face indices were directly collected on a Rigaku RAXIS-PRID diffractometer at ω-scan mode with monochromatized Mo•Kα radiation.

1.2.4 Thermal Analysis

Differential scanning calorimetric (DSC) measurements were performed on a TA DSC Q20 instrument at a heating rate of 10 °C min^{-1} under nitrogen.

1.2.5 Three-Point Bending

Three-point bending tests were carried out on No. 5944 universal materials tester produced by American ITW group Engstrang corporation.

1.2.6 Passive Optical Waveguide

For passive optical waveguide measurements, crystals were irradiated at a tip orthogonal to their long axis with collimated a CW 650 nm LED 500 mW. The diameter of the spot on the crystal was about 1 mm, and the light was collected at the opposite tip of the crystal with an optical fiber connected to an Ocean Optics QE65 Pro spectrometer.

1.2.7 Scanning electron microscopy

Scanning electron microscopy (SEM) images were obtained on a FEI Quanta 450 operated at 5-10 kV.

1.2.8 Nanoindentation

Nanoindentation measurements were conducted using an Agilent Nano Indenter G200 with the CSM method and an XP-style actuator.

1.3 Computational Details

Energy frameworks were performed by CrystalExplorer [S1] using the B3LYP [S2] hybrid functional with the 6-31G (d, p) [S3] basis set, where semiempirical dispersion was included by using the D2 version of Grimme's dispersion. [S4]

Single point energy calculations and noncovalent interaction (NCI) analyses were carried by ORCA [S5,S6] and analyzed by Multiwfn [S7] by using B3LYP with def2-SVP [S8] basis set. To better describe donor-acceptor charge transfer, binding energy calculations were carried by B3LYP with ma-def2-SVP basis set. TD-DFT calculation carried by ORCA analyzed by Multiwfn by using CAM-B3LYP [S9] with def2-SV(P) basis set. The semiempirical dispersion was also included by using D3 version of Grimme's dispersion in all of the calculations. [S10]

Surface energy calculations were implemented by CP2K [S11] using the Perdew–Burke–Ernzerhof (PBE) generalized gradient approximation [S12], where the dispersion correction method selected was the semi-empirical D3 method proposed by Grimme. Input files were created by Multiwfn.

The cutoff energy was set to 1000 Ry. The basis set used for optimization was DZVP-MOLOPT-SR-GTH. The basis set used for energy calculation was TZVP-MOLOPT-GTH. [S13] Bulk energies are computed by adopting the experimentally known space groups and lattice constants, and relaxing the internal atomic positions. Surface energies are calculated by the repeated slab approach with atomic position of the top layer relaxed; other atomic positions were fixed. The vacuum distance of 10 Å was found to be adequate to prevent interaction between isolated molecules. Surface energy ($\boldsymbol{\gamma_s}$) was calculated by the following formula:

$$\gamma_s = \frac{1}{2A} \cdot \left(E_{\text{slab - unrel}} - E_{\text{bulk}}\right) + \frac{1}{A}\left(E_{\text{slab - rel}} - E_{\text{slab - unrel}}\right)$$

Here, A is the area of surface considered, $E_{\text{slab-unrel}}$ and $E_{\text{slab-rel}}$ energies of relax and unrelaxed surface respectively. E_{bulk} is the supercell energy which has same atoms with the slab model.

Table 1. Summary of elastic modulus from references.

Compound Name	Elastic Modulus (Gpa)
N-2,5-dichlorobenzylidine-4-iodo aniline[S14]	8.95
N-4-Chlorobenzylidine-4-fluoro-3-nitroaniline[S14]	6.07
N,N′ -diethyl-1,4,5,8-naphthalenetetracarboxylic diimide[S15]	16.10
copper(II) acetylacetonate[S16]	2–8
(Z)-4-(1-cyano-2-(4-(dimethylamino)phenyl)vinyl)benzonitrile[S17]	0.91

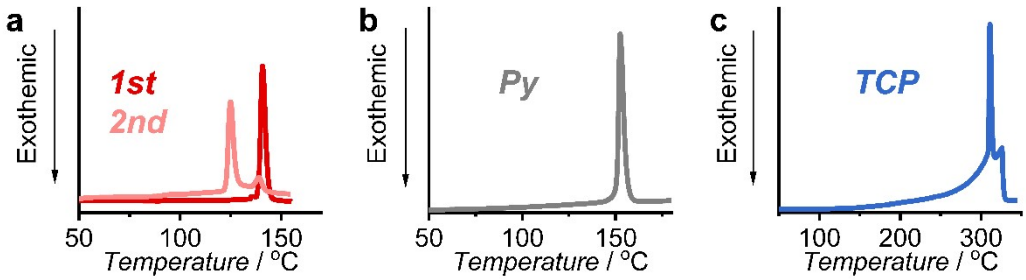

Fig. S1. Differential scanning calorimetric (DSC) curves of the Py-TCP cocrystal (a), pyrene (b) and TCP (c).

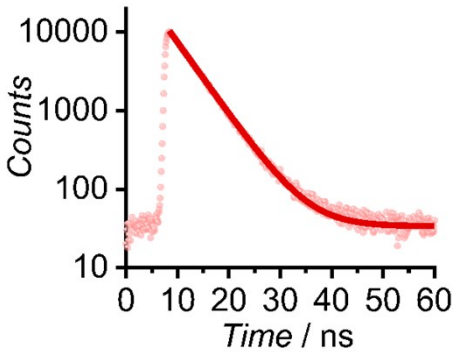

Fig. S2. The fluorescent decay curve of the Py-TCP cocrystal.

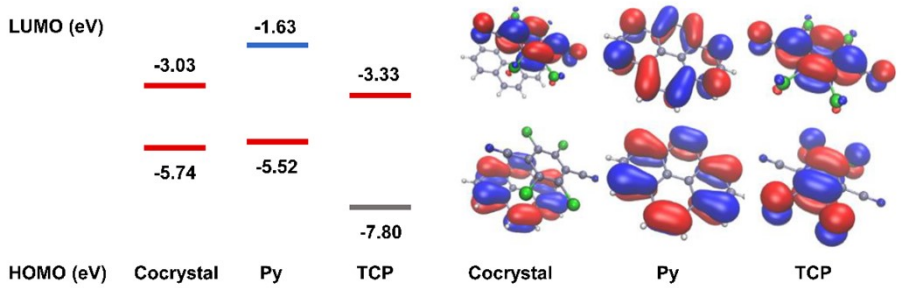

Fig. S3. DFT calculation results of Pyrene, TCP and the Py-TCP cocrystal: energy diagrams, Kohn−Sham HOMOs and LUMOs.

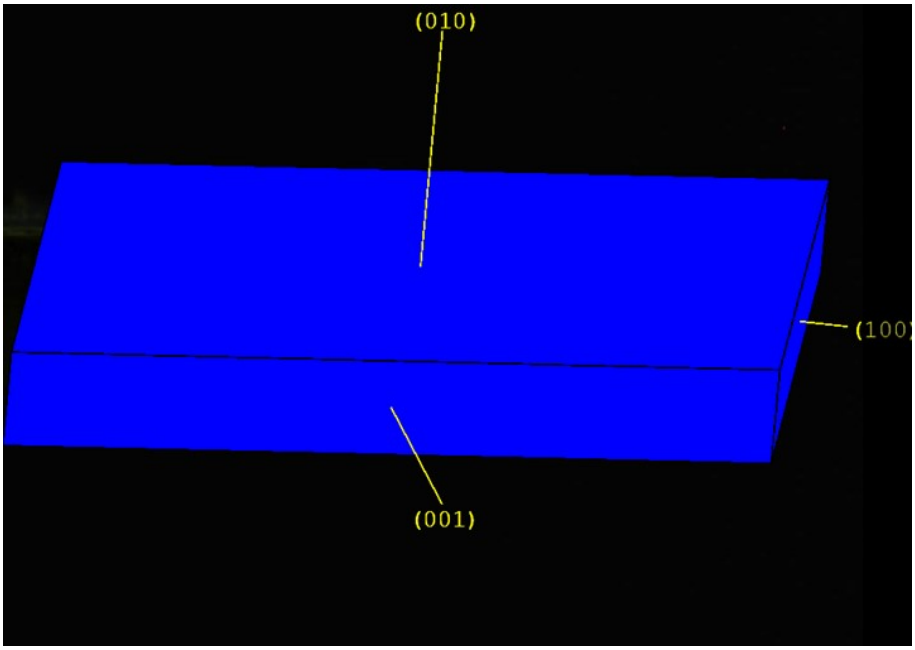

Fig. S4. The determination of crystal faces of the Py-TCP cocrystal by a single crystal X-ray diffraction.

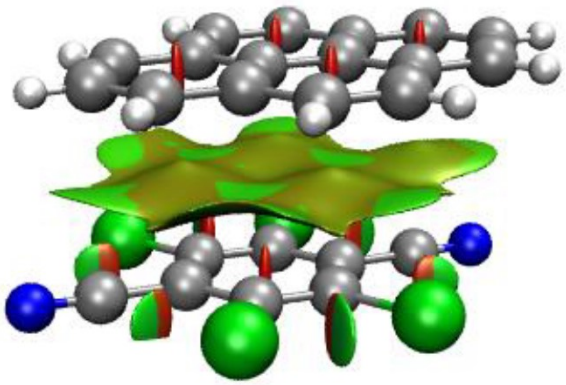

Fig. S5. The NCI analysis of the donor-acceptor interaction in the 1D column of the Py-TCP cocrystal.

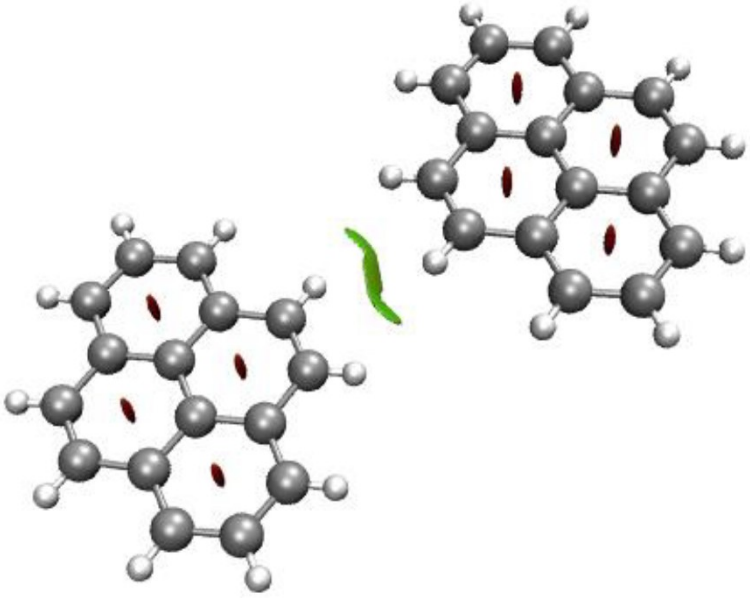

Fig. S6. The NCI analysis of the C-H··· π interaction between 1D columns of the Py-TCP cocrystal.

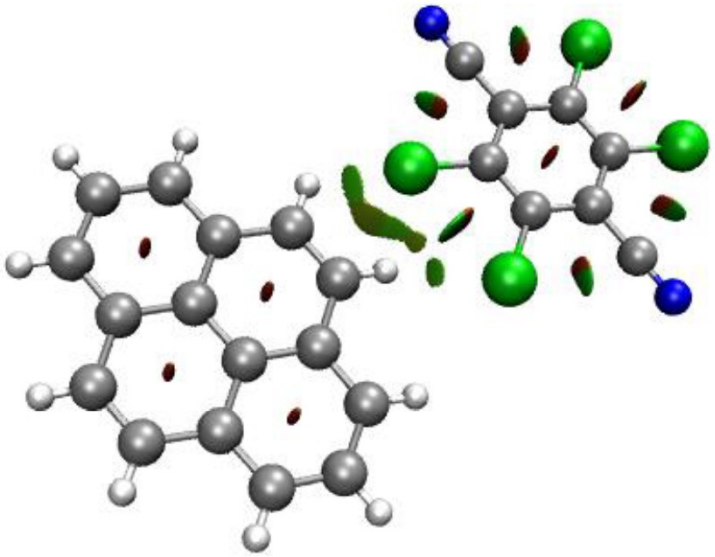

Fig. S7. The NCI analysis of the Cl···H interaction between 1D columns of the Py-TCP cocrystal.

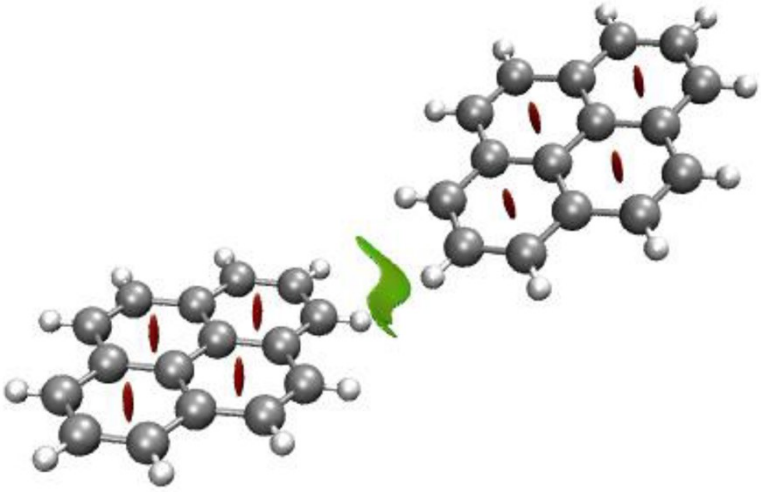

Fig. S8. The NCI analysis of the C-H··· π interaction in the (001) plane of the Py-TCP cocrystal.

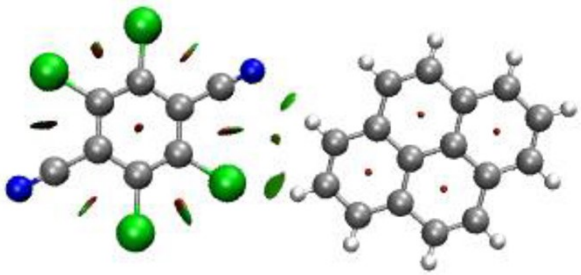

Fig. S9. The NCI analysis of the Cl···H together with the N···H interaction in the (001) plane of the Py-TCP cocrystal.

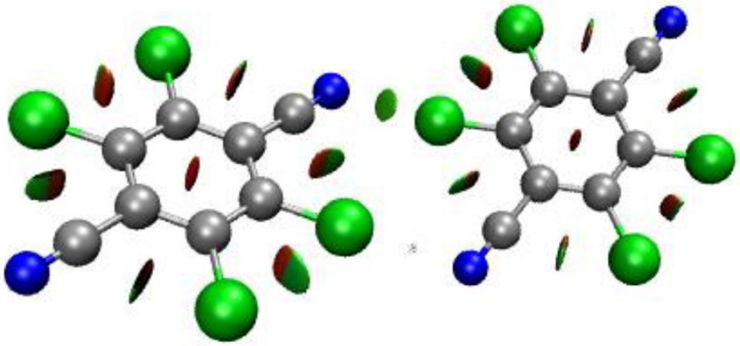

Fig. S10. The NCI analysis of the N···Cl interaction in the (001) plane of the Py-TCP cocrystal.

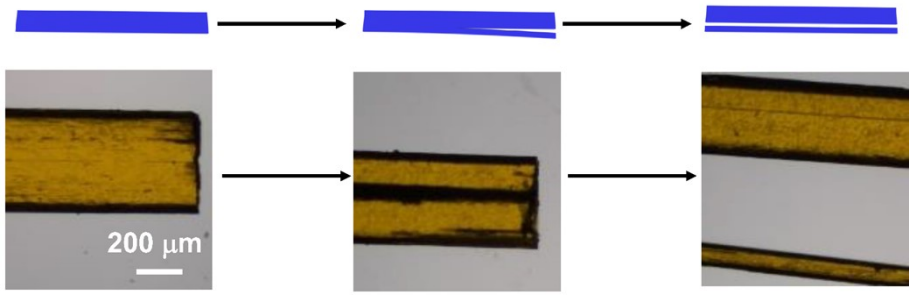

Fig. S11. Cutting processes of the Py-TCP cocrystal monitored by the microscope.

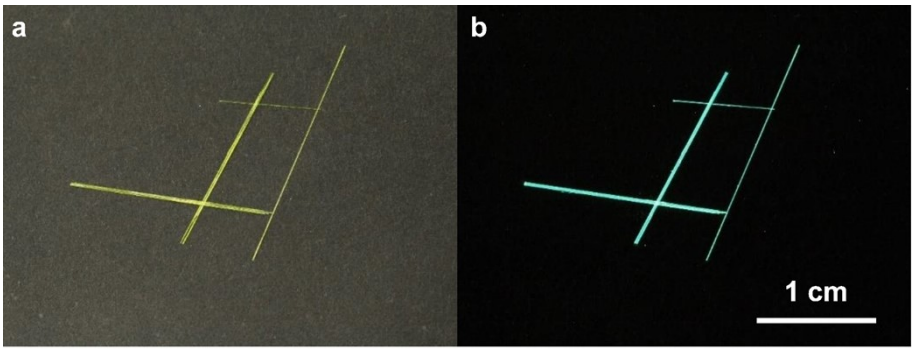

Fig. S12. Photographs of the Py-TFP cocrystal under room light and 365 nm UV light.

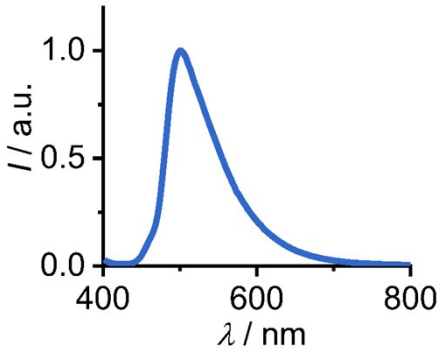

Fig. S13. The emission spectrum of the Py-TFP cocrystal.

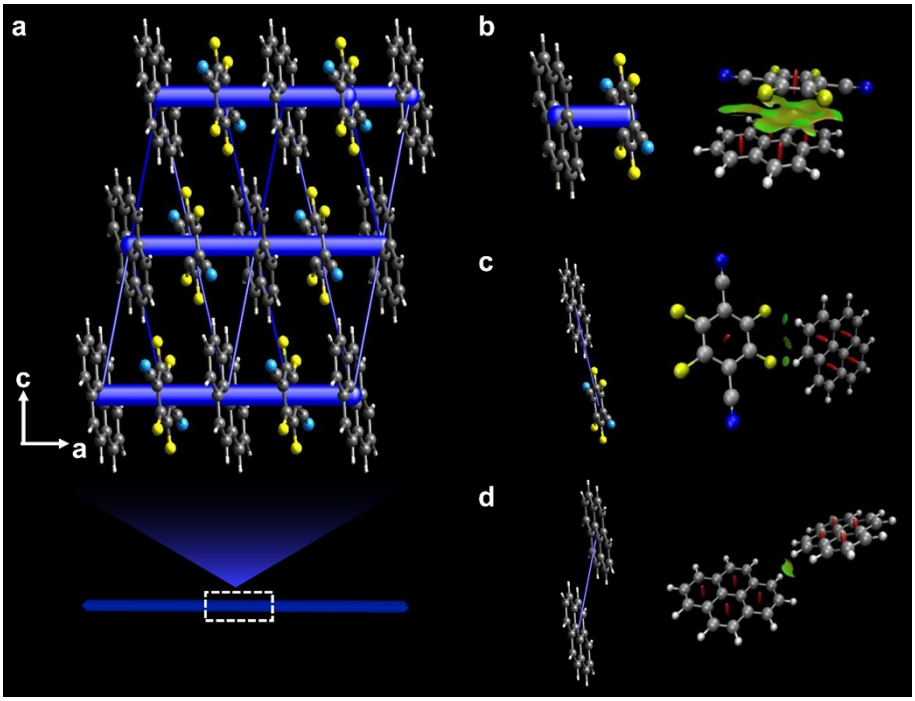

Fig. S14. The energy framework of the Py-TFP cocrystal (a), representative the dimer energy framework and corresponding NCI analyses (b - d).

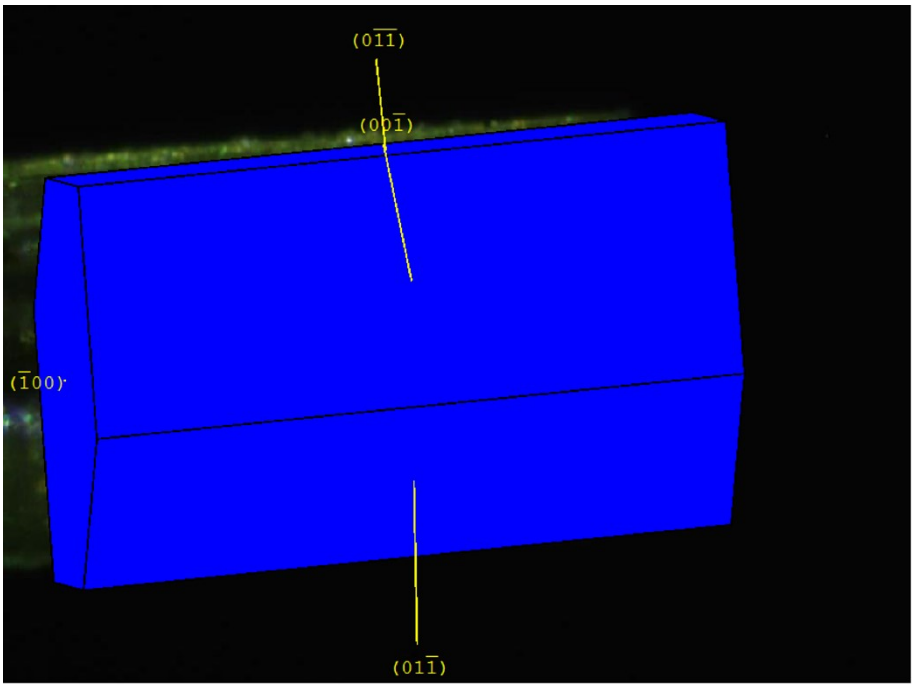

Fig. S15. The determination of crystal faces of the Py-TFP cocrystal by a single crystal X-ray diffraction.

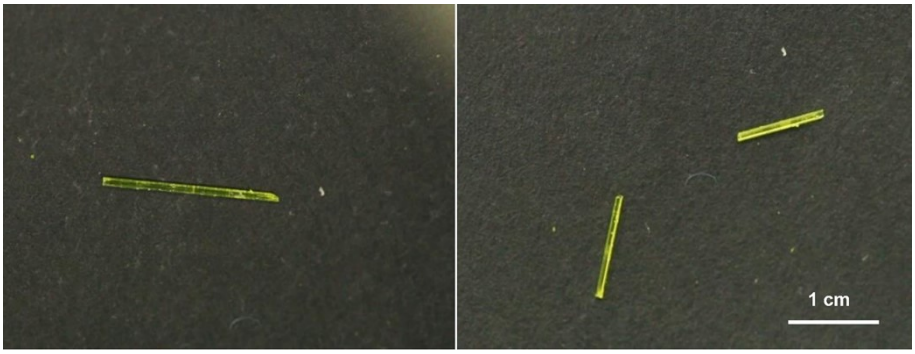

Fig. S16. Photographs of the Py-TFP cocrystal before and after the force applied.

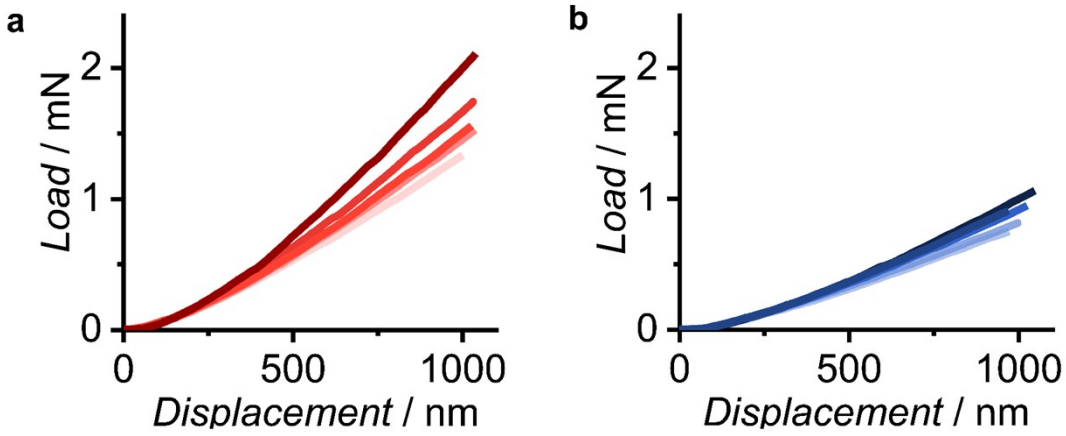

Fig. S17. Load–displacement curves obtained from nanoindentation tests of the Py-TCP cocrystal (a) and the Py-TFP cocrystal (b).

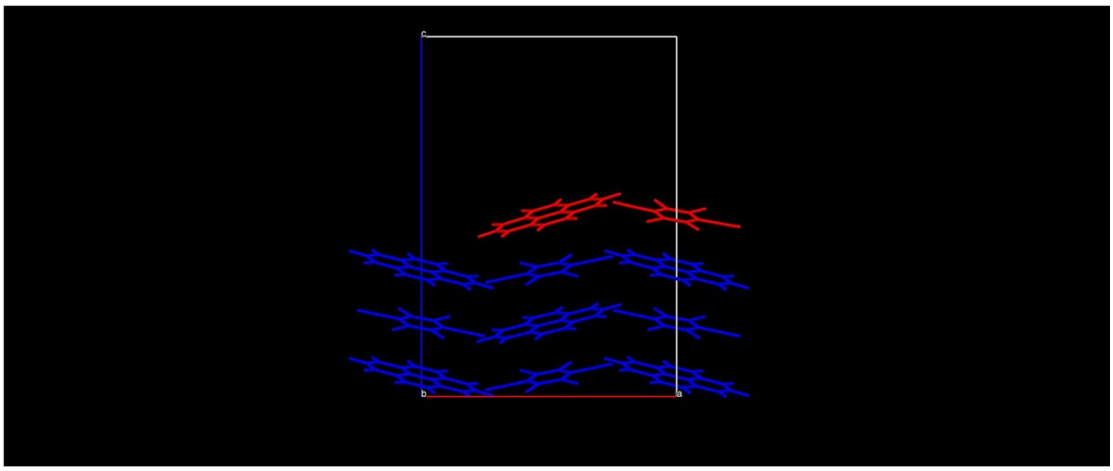

Fig. S18. The slab model used when calculating the surface energy of the (100) plane. Frozen atoms are blue; optimized atoms are red.

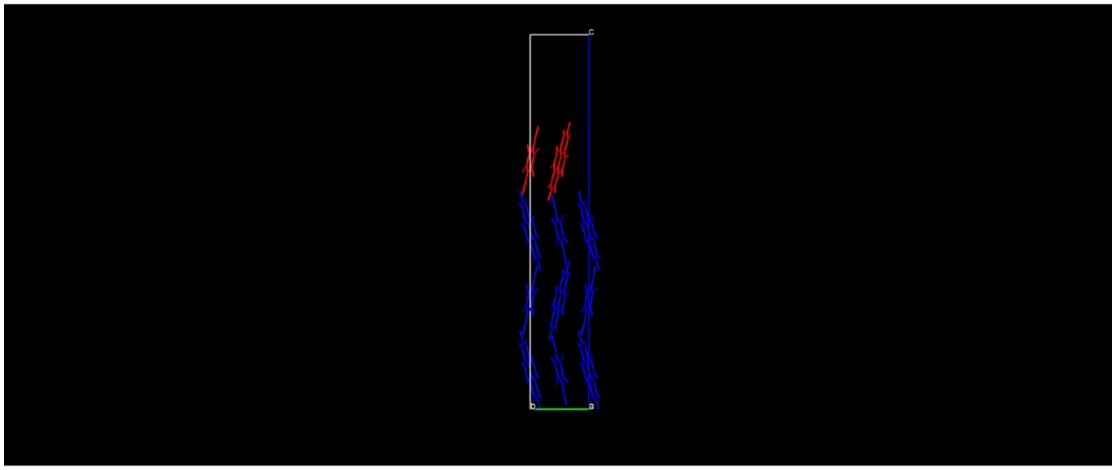

Fig. S19. The slab model used when calculating the surface energy of the (010) plane. Frozen atoms are blue; optimized atoms are red.

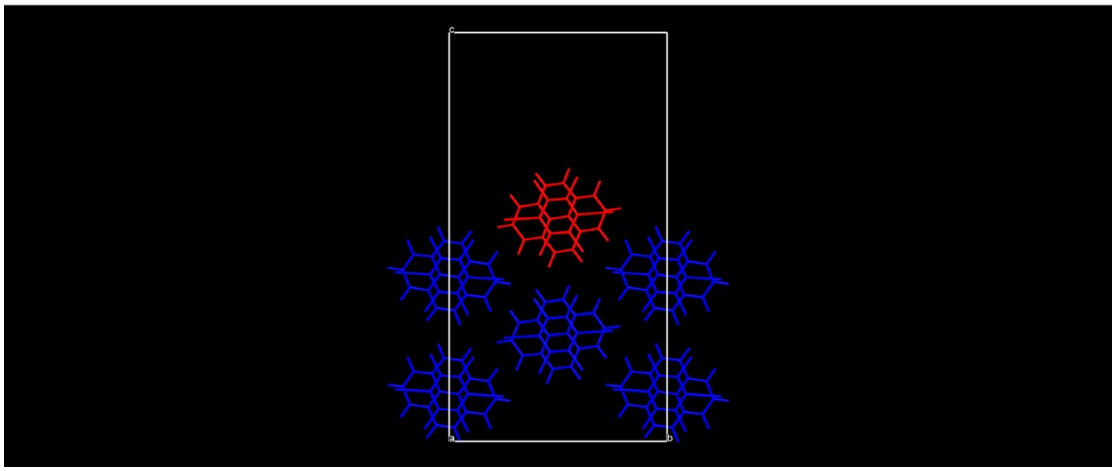

Fig. S20. The slab model used when calculating the surface energy of the (001) plane. Frozen atoms are blue; optimized atoms are red.

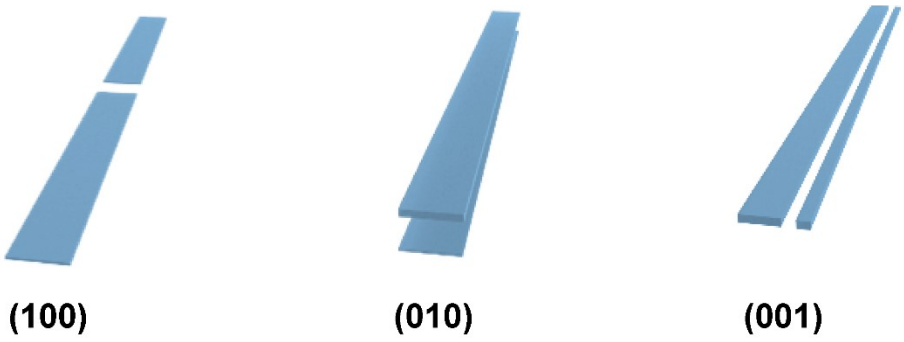

Fig. S21. Schematic illustrations of cleavage surfaces (100), (010) and (001)

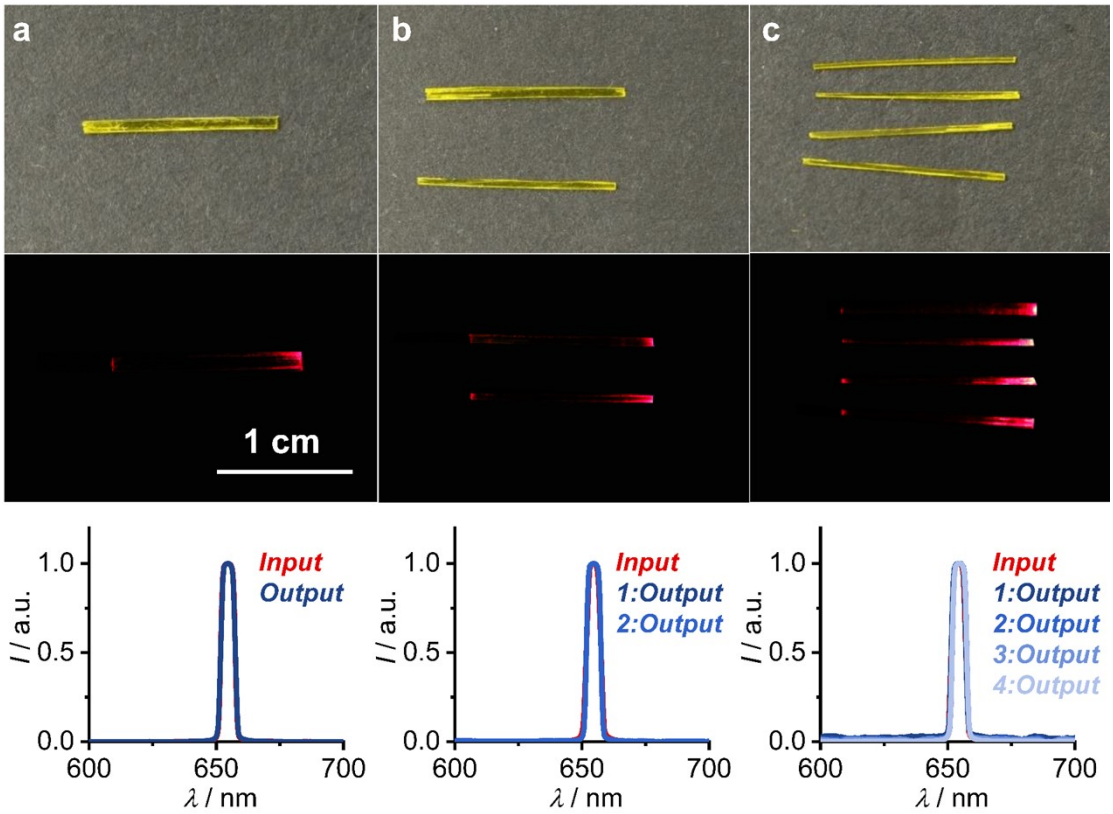

Fig. S22. The transduction of the red light by the Py-TCP cocrystal (a), and the cleavage cocrystal (b, c). And their corresponding normalized spectra of the input LED source and the output light.

Reference

S1 P. R. Spackman, M. J. Turner, J. J. McKinnon, S. K. Wolff, D. J. Grimwood, D. Jayatilaka, M. A. Spackman, *J. Appl. Crystallogr.*, 2021, **54,** 1006-1011.

S2 P. J. Stephens, F. J. Devlin, C. F. Chabalowski, M. J. Frisch, *J. phys. Chem.*, 1994, **98,** 11623-11627.

S3 W. J. Hehre, R. Ditchfield, J. A. Pople, *J. Chem. Phys.*, 1972, **56,** 2257-2261.

S4 S. Grimme, *J. Comput. Chem.*, 2006, **27,** 1787-1799.

S5 F. Neese, *Wiley Interdiscip. Rev.-Comput. Mol. Sci.*, 2012, **2,** 73-78.

S6 F. Neese, *Wiley Interdiscip. Rev.-Comput. Mol. Sci.*, 2018, **8,** 1327.

S7 T. Lu and F. W. Chen, *J. Comput. Chem.*, 2012, **33,** 580-592.

S8 F. Weigend, R. Ahlrichs, *Phys. Chem. Chem. Phys.*, 2005, **7,** 3297-3305.

S9 T. Yanai, D. P. Tew, N. C. Handy, *Chem. Phys. Lett.*, 2004, **393,** 51-57.

S10 S. Grimme, J. Antony, S. Ehrlich and H. Krieg, *J. Chem. Phys.*, 2010, **132,** 154104.

S11 T. D. Kuhne, M. Iannuzzi, M. Del Ben, V. V. Rybkin, P. Seewald, F. Stein, T. Laino, R. Z. Khaliullin, O. Schutt, F. Schiffmann, D. Golze, J. Wilhelm, S. Chulkov, M. H. Bani-Hashemian, V. Weber, U. Borstnik, M. Taillefumier, A. S. Jakobovits, A. Lazzaro, H. Pabst, T. Muller, R. Schade, M. Guidon, S. Andermatt, N. Holmberg, G. K. Schenter, A. Hehn, A. Bussy, F. Belleflamme, G. Tabacchi, A. Gloss, M. Lass, I. Bethune, C. J. Mundy, C. Plessl, M. Watkins, J. VandeVondele, M. Krack, J. Hutter, *J. Chem. Phys.*, 2020, **152,** 194103.

S12 M. Ernzerhof, G. E. Scuseria, *J. Chem. Phys.*, 1999, **110,** 5029-5036.

S13 J. VandeVondele, J. Hutter, *J. Chem. Phys.*, 2007, **127,** 114105.

S14 M. K. Mishra, S. B. Kadambi, U. Ramamurty, S. Ghosh, *Chem. Commun.*, 2018, **54**, 9047-9050.

S15 R. Devarapalli, S. B. Kadambi, C. T. Chen, G. R. Krishna, B. R. Kammari, M. J. Buehler, U. Ramamurty, C. M. Reddy, *Chem. Mat.*, 2019, **31**, 1391-1402.

S16 A. Worthy, A. Grosjean, M. C. Pfrunder, Y. A. Xu, C. Yan, G. Edwards, J. K. Clegg, J. C. McMurtrie, *Nat. Chem.*, 2018, **10**, 65-69.

S17 Z. Q. Lu, Y. P. Zhang, H. Liu, K. Q. Ye, W. T. Liu, H. Y. Zhang, *Angew. Chem. Int.*

Edit., 2020, **59**, 4299-4303.